Unified conversions between total scattering data formalisms

Peter F Peterson,* Dan Olds and Marshall McDonnell

Neutron Scattering Division, Oak Ridge National Laboratory, Oak Ridge, TN, USA.

E-mail: petersonpf@ornl.gov

Abstract

The total scattering method is the simultaneous study of both the real- and reciprocal-space representations of diffraction data. While conventional Bragg-scattering analysis (employing methods such as Rietveld refinement) provides insight into the average structure of the material, pair-distribution function (PDF) analysis allows for a more focused study of the local atomic-arrangement of a material. Generically speaking, a PDF is generated by Fourier transforming the total measured reciprocal space diffraction data (Bragg and diffuse) into a real space representation. However, the details of the transformation employed and, by consequence, the resultant appearance and weighting of the real-space representation of the system often varies between different research communities. As the worldwide total scattering community continues to grow, these subtle differences in nomenclature and data representation have led to conflicting and confusing descriptions of how the PDF is defined and calculated. In this paper, we present a consistent derivation to many of these different forms of the PDF and the transformations required to bridge between them.

1. Introduction

The use of pair-distribution function (PDF) analysis has grown from a specialized technique employed uniquely by the liquids and glasses community (where standard Bragg diffraction analysis was not possible) to a commonly used method in the study of local atomic structure in ordered and disordered crystalline materials. As various material communities have begun to employ PDF analysis, they have refined the methods and developed corresponding analysis software to address the needs of their specific scientific inquiries. The weighting and normalization of different features, either from the measured reciprocal-space data or modeled real-space atomic coordinates, has led to no less than 10 different published forms of real-space functions, which can all claim in one way or another to be analogous to the PDF. Despite being functionally similar, the differences between these varied forms has led to confusion in and across the different user communities. Common variables (e.g. $G(r)$) and terms are defined in similar-but-different ways across disciplines or papers. While this is confusing even for experts in the field, it can be exhaustively daunting for novices.

This contribution aims to untangle many of these semantic and terminological confusions through a consistent derivation of the relationships between many different forms of the PDF. Here, we reintroduce many fundamental concepts and formalisms, and directly relates them to the physical features they represent. Details of the functional forms employed by many PDF analysis software packages are also described. While the equations presented here employ neutron scattering lengths, these derivations are functionally identical for x-rays through replacement of neutron scattering lengths with X-ray form factors. (Juhás *et al.*, 2013)

We note that previous work by Keen (Keen, 2001) went into great detail on the derivation and conversion of different functional forms of the PDF, and is widely cited in the amorphous and liquids community or those employing reverse Monte Carlo

(RMC) methods. This manuscript seeks to follow up and expand on Keen's work by beginning with the conventions of the disordered crystalline material communities (Egami & Billinge, 2012) and bridging to the Keen derivations. Effort has been made in all cases of presenting different PDF formalism to reference both the initial derivations and examples of these formalism in publications.

After a brief explanation of how the simulated data presented was generated, this paper is organized into two derivations with supporting information to lead the reader. Many ancillary details have been moved from the main text into appendices to allow the reader to follow the main text with less distraction. Appendix A provides summaries of the transformations between the various real space functions. Appendix B has a overview of converting from measured intensities to differential cross-sections to act as a starting point for understanding experimental concerns. Appendix C details calculating the normalized Laue term while Appendix D details calculating the number density. Appendix E has a brief overview of partial structure functions.

2. Methods

To illustrate the different functions contained herein, we have simulated neutron nuclear scattering data from the bulk binary oxide MnO (Sasaki *et al.*, 1979), as the negative scattering length of Mn will help emphasize some of the difficulties in interpreting figures and calculating asymptotes. Simulated data from Ar is also included, both as a monotonic example and to highlight the advantages of certain forms for non-crystalline materials. Ar as a liquid is frequently used as a first example in molecular dynamics that should be straightforward for the reader to reproduce.

To generate the presented MnO data, real-space patterns were simulated with PDFgui software(Farrow *et al.*, 2007) using the crystal structure in Table1. Patterns were calculated from r = 0 Å to 160 Å with a bin width of $\delta r = 0.01$ Å.

Table 1. *Summary of structure of MnO used for examples (Sasaki* et al.*, 1979). The structure is* $Fm\overline{3}m$ *with a lattice constant of* $4.446(1)\mathring{A}$

Atom	(x,y,z) (fractional units)	Uiso ($\mathring{A}^2$)
Mn2+	$(0.0, 0.0, 0.0)$	0.617(5)
O2-	$(0.5, 0.5, 0.5)$	0.72(1)

To generate the Ar data, molecular dynamics simulations (MD) were performed using the Large-Scale Atomistic/Molecular Massively Parallel Simulator (LAMMPS) open-source code (Plimpton, 1995; Plimpton, 2018). For all simulations, the system consisted of a cubic simulation cell with 50,000 atoms and a velocity-Verlet-like (Verlet, 1967) time integrator was used with a 1 fs timestep. A Lennard-Jones pair potential with a 15 Å cutoff was used with a tail correction applied, with $\epsilon = 0.238067$ kcal/mol and $\sigma = 3.405$ Å (Yarnell *et al.*, 1973). Initially, the atoms were randomly placed in the box and then force minimized with a force tolerance of 10^{-8} kcal/ (mole Å). To produce the real and reciprocal space patterns, canonical (NVT) ensemble simulation were carried out with T=86.56 K and $\rho = 0.02138$ atoms/$\mathring{A}^3$ to reproduce previous neutron diffraction and MD results (Yarnell *et al.*, 1973). A Nosé-Hoover style thermostat (Nosé, 1984; Hoover, 1985) was used to keep constant temperature with a relaxation time of 0.1 ps. For the isothermal compressibility calculations, isobaric-isothermal (NPT) simulations were carried out at the same temperature from the NVT simulation but with different pressures. A Nosé-Hoover style barostat (Nosé, 1984; Hoover, 1985) was used to keep constant pressure with a relaxation time of 1 ps.

In both the case of MnO and Ar, reciprocal space data was generated from the real-space simulated data through the use of custom python codes, which performed an inverse Fourier transform. Resultant data is scaled such that forward transforms recreate desired PDF precisely.

3. Reciprocal space functions

In this work, we begin our derivation assuming data in the form of the fully corrected and normalized intensity, $I(Q)$. The details of the reduction protocols from the initial measured intensity to this fully reduced format can be found in Appendix B. One straightforward method of directly relating a set of atomic coordinates to $I(Q)$ is through the Debye equation (Debye, 1915). Modifying Debye's original formalism slightly to include the effects of thermal atomic displacements through a Debye-Waller term, this is written as

$$I(Q) = \sum_{\nu\mu} b_{coh,\nu} b_{coh,\mu} \frac{\sin(Qr_{\nu\mu})}{Qr_{\nu\mu}} \exp\left(\frac{-\sigma_{\nu\mu}^2 Q^2}{2}\right) \tag{1}$$

where $b_{coh,\nu}$ is the coherent scattering length of the ν atom and $r_{\nu\mu} = |\vec{r_\nu} - \vec{r_\mu}|$ is the interatomic pair-wise vector (Farrow & Billinge, 2009; Page *et al.*, 2011; Lovesey, 1986). Note that when defined only through isotropic atomic displacement parameters (commonly referred to as U_{iso}), $\sigma_{\nu\mu}$ the Debye-Waller term can be written as (Jeong *et al.*, 1999; Proffen & Billinge, 1999; Jeong *et al.*, 2003)

$$\sigma_{\nu\mu} = \sqrt{\sigma_\nu^2 + \sigma_\mu^2} \tag{2}$$

where σ_ν is the amplitude of the uncorrelated thermal motion. **This relationship is more complicated in the case of anisotropic atomic displacement (reference needed), but its effect on the normalized intensity is similar: it exponentially dampens the intensity of scattering at high Q. There is a bonus section 4.1 that has more of the details. Reference Old's Acta Crysta 2018?**

Another useful form of the normalized and corrected scattering data is the so called structure function, $S(Q)$. As we will soon see, this form of the scattering data is often employed in the generation of many atomic pair-pair representations of the data, which accounts for its widespread description in past work (Billinge & Egami, 1993;

Keen, 2001; Peterson *et al.*, 2003; Farrow & Billinge, 2009; Page *et al.*, 2011; Olds *et al.*, 2015; Yarnell *et al.*, 1973) where details of the derivation can be found. The structure function is related to the normalized $I(Q)$ function through the relationship

$$S(Q) = \frac{I(Q)}{N\langle b_{coh}\rangle^2} - \frac{\langle b_{tot}^2\rangle - \langle b_{coh}\rangle^2}{\langle b_{coh}\rangle^2}, \tag{3}$$

where N is the number of atoms in the system, $\langle b_{tot}\rangle$ is the average total scattering power of the system, $\langle b_{coh}\rangle$ is the average coherent scattering power of all atoms in the sample, and η accounts for the contributions from the compressibility of the sample.

Although this may seem an intimidating conversion at first, note that $S(Q)$ is functionally just the normalized scatter, $I(Q)$, which has been scaled by a constant factor related to the sample composition, and then shifted slightly by a factor representing the incoherent scattering contributions to the measured data.

The second term in equation 3 contributes a constant factor called the normalized Laue monotonic diffuse scattering term. This Laue term is often written simply as L, where

$$L = \frac{\langle b_{tot}^2\rangle - \langle b_{coh}\rangle^2}{\langle b_{coh}\rangle^2}. \tag{4}$$

Physically, L arises from the imperfect cancellation of intensity at the destructive interference condition when atomic sites are occupied by atoms of different scattering strength. Thus, L contributes an incoherent background even in the case of perfect coherent scattering (Farrow & Billinge, 2009). It is zero in the case of single element scattering (though not strictly so for neutron scattering, since a mix of isotopes often comprises naturally abundant elemental samples). Appendix C demonstrates the proper way of calculating L for a number of examples. The limits of the function are thus relatively straightforward, and when incorporated into equation 3 results in

the limits of $S(Q)$ being

$$\lim_{Q\to\infty} S(Q) = 1. \tag{5}$$

and from Lovesey equation 5.34

$$\lim_{Q\to 0} S(Q) = \eta \tag{6}$$

Note that the trend of $S(Q)$ below the first Bragg peak is to approach this limit linearly. η is unitless and proportional to the isothermal compressibility of the sample, such that it is often negligible (Bhatia & Thornton, 1970; Wagner, 1985; Keen, 2001) (as shown in examples in table 2). Explicitly, η is defined as

$$\eta = \rho_0 \kappa k_B T = k_B T \left(\frac{\partial \rho}{\partial P}\right)_T = 1 + \rho_0 \int_0^\infty 4\pi r^2 [g(r) - 1] dr \tag{7}$$

where the last equality for η is the compressibility equation with $g(r)$ defined later in Eq. 21. κ is the isothermal compressibility (equal to the inverse of the bulk modulus, K_0), ρ_0 is the number density, k_B is Boltzman's constant, and P is pressure. The isothermal compressibility can be calculated as

$$\kappa = -\frac{1}{V}\left(\frac{\partial V}{\partial P}\right)_T = \frac{\langle \sigma_v^2 \rangle}{V k_B T} = \frac{1}{\rho_0 k_B T}\left[1 + \rho_0 \int_0^\infty 4\pi r^2 [g(r) - 1] dr\right] \tag{8}$$

where σ_v^2 is the variance of the volume.

The low-Q limit of $S(Q)$ assumes the sample is infinitely large, with no correlated features larger than the unit cell. In cases where nanostructured features exist (such as materials where small-angle scattering is present) the measured low-Q behavior will be different (Farrow & Billinge, 2009; Olds *et al.*, 2015). The value of η is considered negligible for solids around room temperature (Egelstaff, 1992; Wang *et al.*, 2014).

The kernel of the Fourier transform, often referred to as the reduced total scattering structure function (Egami & Billinge, 2012) is defined as

$$F(Q) = Q[S(Q) - 1]. \tag{9}$$

In practice, it can be useful to plot measured data as $F(Q)$, as this can highlight issues at high-Q, such as noise and resolutions artifacts, that can ultimately have dramatic effects on the resultant real-space PDF (Olds *et al.*, 2018).

Note that in the derivations of Keen(Keen, 2001), a variable $F(Q)$ is presented, which although similar, is different than the form defined herein (and employed by the disordered materials community). This alternative function, here referred to as $F_K(Q)$, is scaled by $\langle b_{coh}\rangle^2$, and not by Q. Thus, these three reciprocal space function are related as

$$F_K(Q) = \langle b_{coh}\rangle^2[S(Q)-1] = \frac{\langle b_{coh}\rangle^2}{Q}F(Q) \tag{10}$$

Relating $F_K(Q)$ to the normalized, corrected measurement is

$$F_K(Q) = \frac{I(Q)}{N} - \langle b_{tot}^2\rangle + \langle b_{coh}\rangle^2\eta \tag{11}$$

Similarly,

$$F(Q) = \frac{Q}{\langle b_{coh}\rangle^2}\left[\frac{I(Q)}{N} - \langle b_{tot}^2\rangle + \langle b_{coh}\rangle^2\eta\right] \tag{12}$$

A visual comparison of these three functions is shown for the case of MnO in figure 1, and for the case of Ar in figure 2. A summery of the the limiting behaviors of $I(Q)$, $S(Q)$, $F(Q)$, and $F_K(Q)$ can be found in table 3.

Table 2. *Table of η for the materials chosen at room temperature (300 K). The bulk modulus for MnO is taken from (Zhang, 1999).*

Material	$K_0 = 1/\kappa$ (GPa)	ρ_0 (atoms/Å^3)	η
Ar	0.552	0.02138	0.046
MnO	148	0.0455	0.0013

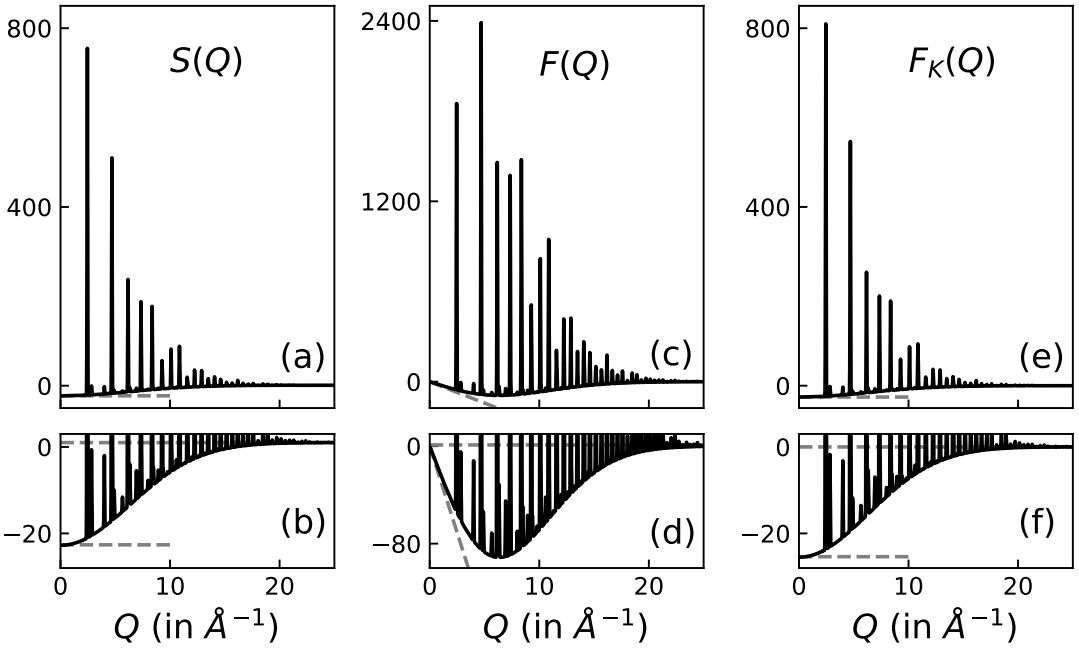

Fig. 1. Comparison of reciprocal space representations of MnO total scattering data. (a) and (b) are $S(Q)$, (c) and (d) are $F(Q) = Q[S(Q) - 1]$, and (e) and (f) are $F_K(Q) = \langle b_{coh} \rangle^2 [S(Q) - 1]$. The upper plots show an overview of the various functions while the asymptotes are highlighted by lower plots with dashed lines. In this case, $\langle b_{coh} \rangle^2 = 1.074 fm^2$ so the difference between $S(Q)$ and $F_K(Q)$ appears to be only a vertical shift of one (1). This is purely coincidental. **Check low-Q limit in figures!**

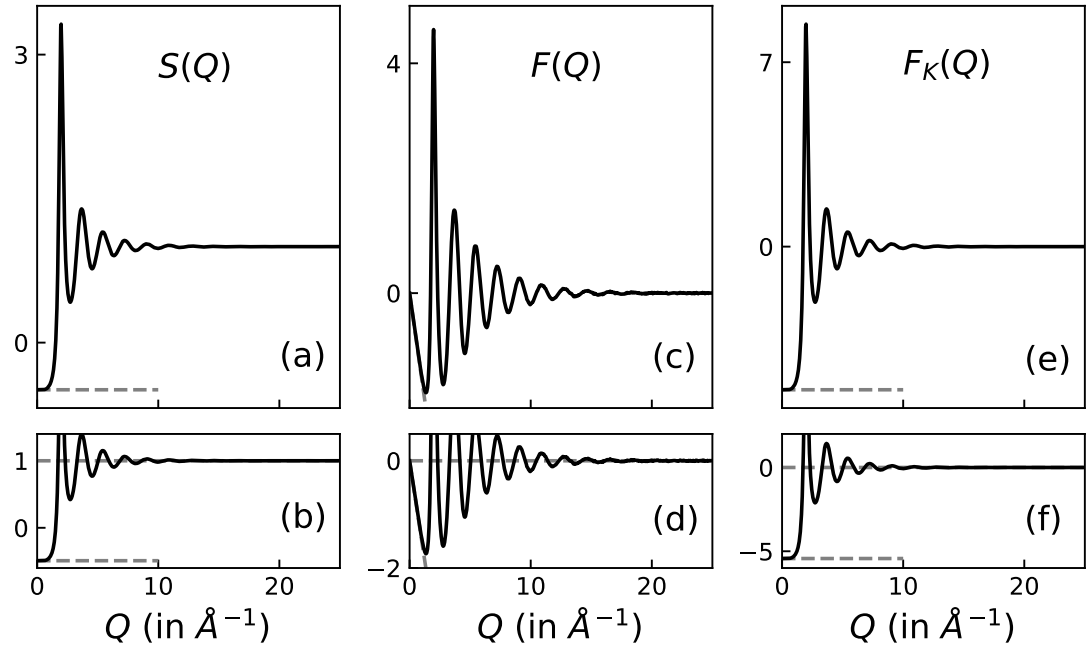

Fig. 2. Comparison of reciprocal space representations of Ar total scattering data. (a) and (b) are $S(Q)$, (c) and (d) are $F(Q) = Q[S(Q)-1]$, and (e) and (f) are $F_K(Q) = \langle b_{coh}\rangle^2[S(Q)-1]$. The upper plots show an overview of the various functions while the asymptotes are highlighted by lower plots with dashed lines. **Check low-Q limit in figures!**

Table 3. *Limits of reciprocal space functions. Like radians, atoms is normally not listed as a unit, but this table is explicitly mentioning it for added clarity.* ***Are units in first line correct?***

function	low-Q behavior	high-Q behavior	units
$I(Q)$	$N\left(\langle b_{coh}\rangle^2(\eta-1)+\langle b_{tot}^2\rangle\right)$	$N\langle b_{tot}^2\rangle$	barn · atom
$S(Q)$	η	1	unitless
$F(Q)$	$(\eta-1)Q=0$	0	Å^{-}1
$F_K(Q)$	$\langle b_{coh}\rangle^2(\eta-1)$	0	barn

4. Real space distribution functions

A pair distribution function (PDF) is a general term for a function that describes the distribution of distances between pairs of objects contained in a given volume. Mathematically, it is described as the probability of finding an object v at a distance r from another object u, with u taken as the origin of coordinates. When defined

independent of origin, this is termed a radial distribution function, an entity that finds prevalent use as a descriptor for the atomic structure of amorphous, liquid, and (increasingly) disordered crystalline materials.

In this section, we derive and relate a number of different functions which describe real-space atomic pair-pair correlations in one method for structural determination or another. We begin by defining a configuration of N atoms arranged such that each atom has a position defined through the vector $\vec{r_\nu}$. The interatomic distance between any pair of atoms, ν and μ, is thus $r_{\nu\mu} = |\vec{r_\nu} - \vec{r_\mu}|$.

An unweighted radial distribution function, $R_u(r)$ can be constructed through the sum of Dirac delta functions, δ, which describe the full set of these pair-pair distances (of which there will be $N(N-1)/2$ total pairs), can be written as

$$R_u(r) = \frac{1}{N} \sum_{\nu\mu} \delta(r - r_{\nu\mu}). \tag{13}$$

The radial PDF can be calculated directly from physical measurements, including light scattering, electron diffraction, x-ray diffraction, and neutron diffraction. To account for scattering powers of atoms, one must include the normalized form of the contributing atoms' scattering length. This results in the weighted radial distribution function, $R(r)$, defined as

$$R(r) = \frac{1}{N} \sum_{\nu\mu} \frac{b_{coh,\nu} b_{coh,\mu}}{\langle b_{coh} \rangle^2} \delta(r - r_{\nu\mu}). \tag{14}$$

Note that in the case of monotomic systems, the weighting prefactor will become unity, and $R(r)$ simplifies to become identical to $R_u(r)$. The radial distribution is zero at distances smaller than the minimum distance between atoms, and assuming the configuration of atoms is infinite (or has periodic boundaries), approaches infinity as the distance increases.

A similar formalism often encountered is the atomic number density, $\rho(r)$, which is the radial distribution function normalized by the surface area of a sphere of radius,

r, such that

$$\rho(r) = \frac{R(r)}{4\pi r^2}. \tag{15}$$

This atomic number density can be directly related to $S(Q)$ through the following pair of transforms (Warren, 1990; Billinge, 1992).

$$S(Q) - 1 = \frac{4\pi}{Q} \int_0^\infty [\rho(r) - \rho_0] r sin(Qr) dr \tag{16}$$

and

$$\rho(r) = \rho_0 + \frac{1}{2\pi^2 r} \int_0^\infty Q[S(Q) - 1] sin(Qr) dQ \tag{17}$$

I don't know what math these references are talking about anymore : (Kodama *et al.*, 2006; Gilbert, 2008; Farrow & Billinge, 2009).

Arguably, the most common form of the PDF encountered in the ordered and disordered crystalline community is the reduced pair-distribution function, $G(r)$, which is defined in relation to the atomic pair distribution function as

$$G(r) = 4\pi r[\rho(r) - \rho_0 \gamma_0(r)], \tag{18}$$

where ρ_0 is the average number density of N atoms in the volume V such that $\rho_0 = N/V$, and $\gamma_0(r)$ is the characteristic shape function or nanoparticle form factor(Guinier & Fournet, 1955; Azaroff, 1968; Farrow & Billinge, 2009; Olds *et al.*, 2015) which describes any finite size effects not explicitly included in $\rho(r)$. In cases of bulk materials, $\gamma(r) = 1.0$. This reduced pair-distribution function can be generated from reciprocal space data via the Sine transform of $F(Q)$, such that

$$G(r) = \frac{2}{\pi} \int_0^\infty F(Q) sin(Qr) dQ \tag{19}$$

and the corresponding relationship

$$F(Q) = \int_0^\infty G(r) sin(Qr) dr. \tag{20}$$

This is probably a good point to talk about the use of $G(r)$, functionally, and cite some of it's more high-profile papers.

An alternative formalism of the PDF is the so-called pair density function, $g(r)$, is often encountered in studies of amorphous and liquid materials. The pair density function is functionally identical to the atomic number density, $\rho(r)$, however it has been scaled by the average number density, resulting in the relationship

$$g(r) = \frac{\rho(r)}{\rho_0} \tag{21}$$

such that $g(r)$ has a low-r limit of 0, and a high-r limit of 1.

If beginning with a model atomic configuration where atomic species are known, one may construct an atomic-species specific pair density function often referred to as partial PDFs. The derivation of so-called Faber-Ziman partial structure factors is presented in detail in Appendix E. It is suffienct here to understand that the weighted sum of the partial PDFs will result in the pair density function, such that

$$g(r) = \sum_{\nu} \sum_{\mu} W_{\nu\mu} g_{\nu\mu}(r) \tag{22}$$

where $W_{\nu\mu}$ is the associated weighting factor. Different communities employ different normalization schemes for the weighting factors, $W_{\nu\mu}$. Herein, we normalize them such that $\sum_{\nu} \sum_{\mu} W_{\nu\mu} = 1$ unless explicitly noted otherwise.

One of the greatest forms of confusion accross PDF communities can be the differences between the reduced pair distribution function, $G(r)$, and the total radial distribution function, which is often also labeled $G(r)$. For clarity, we here refer to the total radial distribution function as $G_K(r)$. This form of the PDF is conventionally constructed from the sum of all partials, $g_{\nu\mu}(r)$, weighted according to concentration of atomic species, c, and associated coherent scattering power, b_{coh}, such that

$$G_K(r) = \sum_{\nu} \sum_{\mu} c_{\nu} c_{\mu} b_{coh,\nu} b_{coh,\mu} \left[g_{\nu\mu}(r) - 1 \right]. \tag{23}$$

This form of the PDF is most often something something. Note that despite sharing a common variable name, $G_K(r)$ behaves significantly differently from $G(r)$, as they are related by

$$G_K(r) = \frac{\langle b_{coh} \rangle^2}{4\pi\rho_0} \frac{G(r)}{r}. \tag{24}$$

Is there a reason we don't show $G_K(r)$ in any of the plots?

There exists a functionally similar form the the crystalline communities PDF referred to as the differential correlation function, $D(r)$ (Tucker *et al.*, 2007; Tucker *et al.*, 2017). This form of the PDF is curiously identical to $G(r)$ apart from a constant scaling factor such that

$$D(r) = \langle b_{coh} \rangle^2 G(r). \tag{25}$$

Often, it has been incorrectly stated that $D(r)$ is the same as $G(r)$. Although this may work for small-box modeling programs which employ a scale factor (such that $D(r)$ data can be used just as readily as $G(r)$ data), the large-box modeling approaches that rely on absolutely normalized data will be adversely effects by such an assumption.

Adding further confusion to the mix, there exists a total correlation function, $T(r)$ (Soper, 1989; Hannon *et al.*, 1990) , which is related to some of these other forms as

$$T(r) = D(r) + T^0(r) = \langle b_{coh} \rangle^2 4\pi r\rho(r) = \frac{\langle b_{coh} \rangle^2}{r} R(r). \tag{26}$$

Where $T^0(r) = 4\pi r\rho_0$. Clearly, the community has lost its' mind. **I'd love to leave this assessment in - Pete**

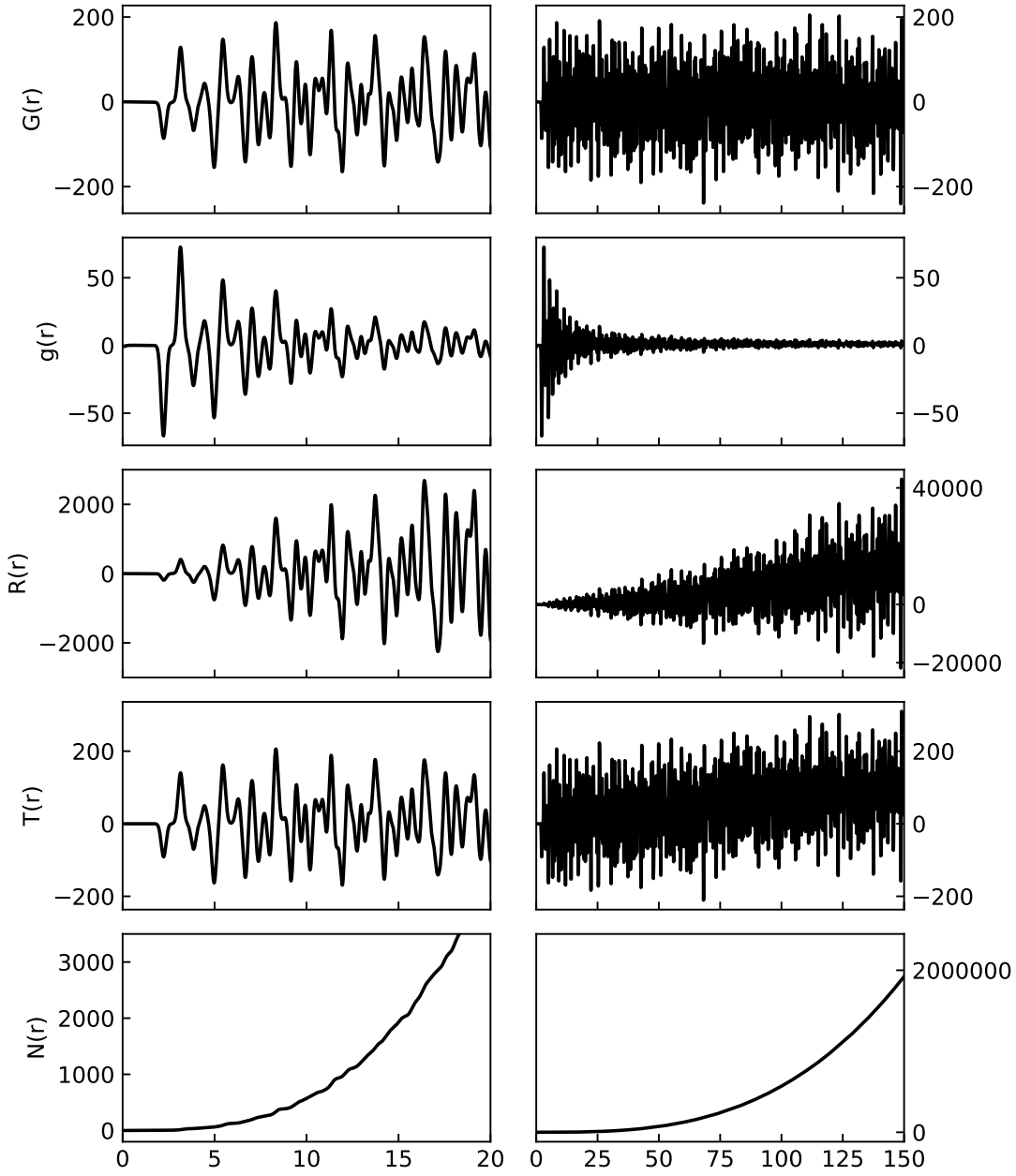

Fig. 3. Comparison on long range behavior of different real-space functions for MnO.

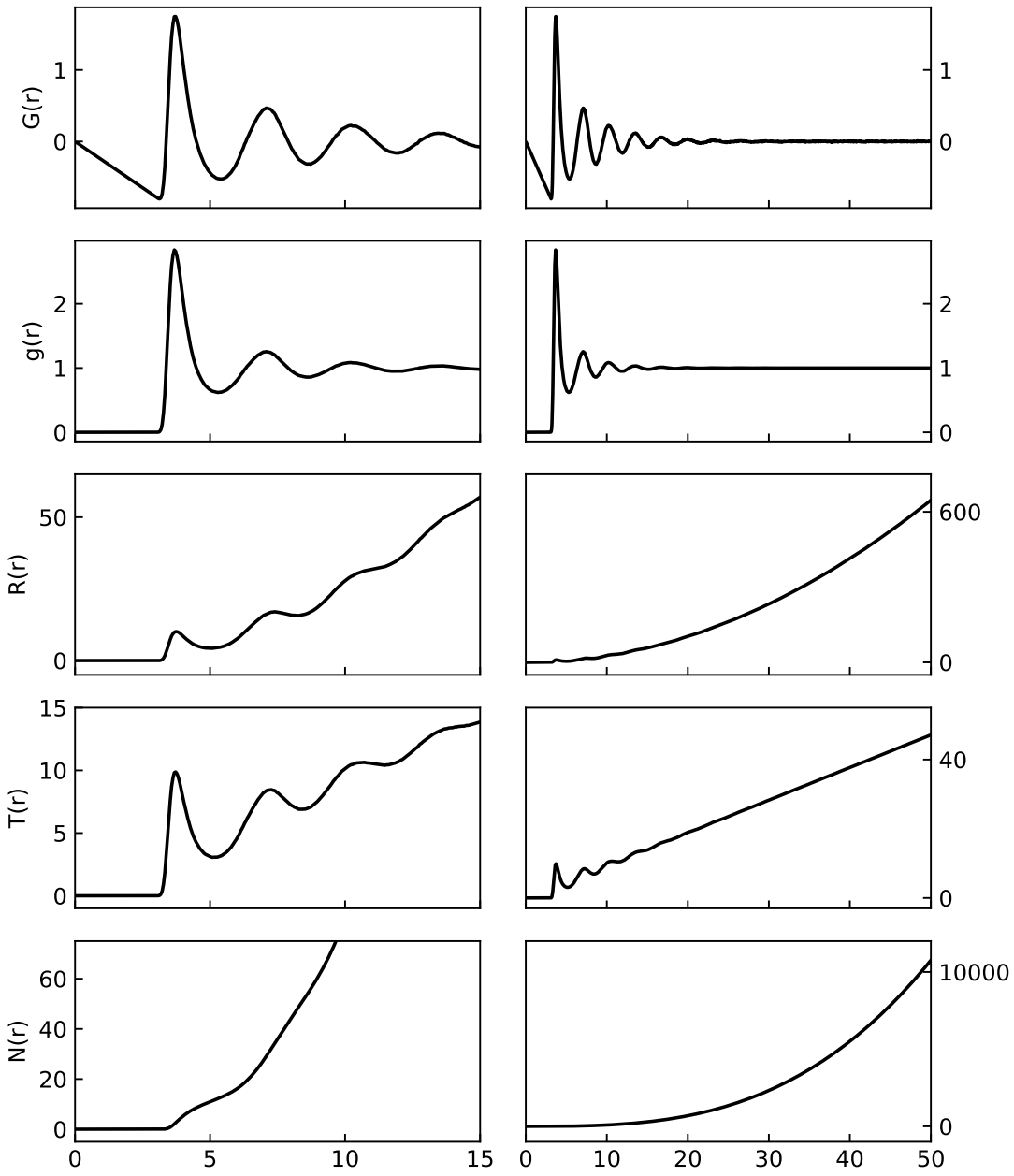

Fig. 4. Comparison on long range behavior of different real-space functions for Ar.

Figures 3 and 4 show a comparison of $G(r)$, $g(r)$, and $R(r)$. For liquids and amorphous materials, the pair density function, $g(r)$ emphasizes the shorter range order. The reduced pair-distribution function, $G(r)$, shows the correlation of atoms over a

long range. Finally, the radial distribution function, $R(r)$, is by far the conceptionally easiest to understand even if it is not as useful because it emphasizes the long range correlations.

Table 4. *Limits of real space functions. Note that for materials with long range order (i.e. crystalline), the high-r behavior is often obscured by the peaks in the distribution function. Like radians, atoms is normally not listed as a unit, but this table is explicitly mentioning it for added clarity.*

function	low-r behavior	high-r behavior	units
$G(r)$	$-4\pi\rho_0 r$	0	atom / Å^2
$g(r)$	0	1	unitless
$R(r)$	0	$4\pi\rho_0 r^2$	atom / Å
$\rho(r)$	0	ρ_0	atom / Å^3
$G_K(r)$	$-\langle b_{coh}\rangle^2$	0	barn
$D(r)$	$-4\pi\rho_0\langle b_{coh}\rangle^2 r$	0	barn $\cdot$ atom / Å^2
$T(r)$	0	$4\pi\rho_0\langle b_{coh}\rangle^2 r$	barn $\cdot$ atom / Å^2
$N(r)$	0	$\propto r^3$	atom

Finally, a PDF data is often enterprited using coordination number, $N(r)$. This is the number of atoms between r_{min} and r_{max}. The coordination number is described mathematically in terms of the partial pair density functions (Soper, 2010)

$$N_{\nu\mu}(r_{min}, r_{max}) = 4\pi\rho_0 c_\mu \int_{r_{min}}^{r_{max}} r^2 g_{\nu\mu}(r) dr \tag{27}$$

which explicitly does not include the scattering lengths. A very related function is the accumulation of this summed over all atoms

$$N(r) = 4\pi\rho_0 \sum_{\nu\mu} c_\mu \int_0^r (r')^2 g_{\nu\mu}(r') dr' \tag{28}$$

Note that coordination number is not weighted by scattering lengths, such that it cannot be easily transformed to other real space without employing partial PDF functions. For the full list of conversions between the many forms of the PDF, see Appendix A.

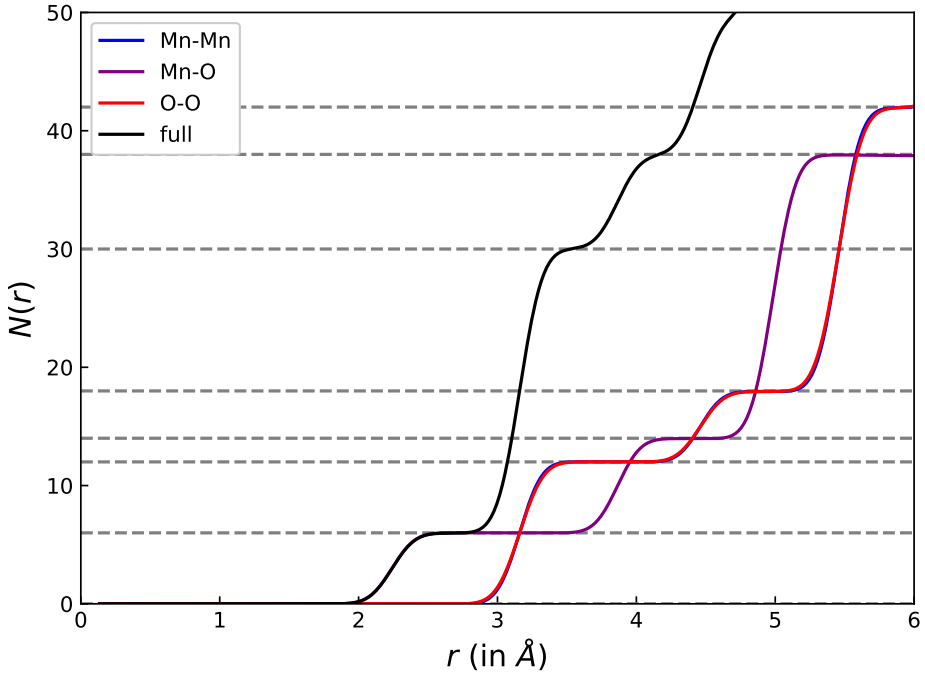

Fig. 5. Accumulated correlation number for MnO plotted with its partials. The partial and full coordination numbers are marked with dashed lines. Note that the partial coordination number for Mn-Mn and O-O are identical due to symmetry, but the isotropic thermal parameters, Uiso, are different which is visible near the plateaus in the Mn-Mn and O-O partials.

4.1. Something about correlated motion

I'm not sure where this belongs in the paper. Probably in a little section about thermal parameters and instrument effects, but not inline with the definitions of the various PDFs. -Dan

This term is often modified by a local correlated motion term, δ_1 or δ_2, which accounts for correlated motion between nearby atoms through effectively lowering this Debye-Waller term at low-r. Similarly, instrument resolution effects can lead to an apparent increase in the Debye-Waller effect at high-r. The correlated motion can be described as an r-dependence of the form (Thorpe *et al.*, 2002; Qiu *et al.*, 2004; Farrow

et al., 2016)

$$\sigma(r) = \sigma_{\nu\mu}\sqrt{1 - \frac{\delta_1}{r} - \frac{\delta_2}{r^2} + Q_{broad}^2 r^2} \tag{29}$$

where $\sigma_{\mu\nu}$ is the initial Debye-Waller term, δ_1 and δ_2 are the correlated motion terms (as linear or squared terms) and Q_{broad} is the instrument resolution function.

5. Conclusions

This paper has shown the relations between all 8 real space distribution functions. Hopefully it has made clearer why some of these forms coexist. In the authors' opinion, it is time to finally reduce the number of real space distribution functions that are in common use. Since different forms emphasize different behavior we suggest reducing the number to 2, $G(r)$ and $g(r)$. These functions allow for the emphasis of the low-r behavior in $g(r)$ and consistent behavior over a range of distances with $G(r)$.

Less controversially, the authors suggest that other authors are overly clear in which functions they are presenting. In any publication describe your reciprocal space function in terms of $S(Q)$. For example "figure 12 show the structure function, $F(Q) = Q[S(Q)-1]$." Similarly, describe your real space functions in terms of $\rho(r)$. For example "we fit the pair distribution function, $G(r) = 4\pi[\rho(r) - \rho_0]$."

Appendix A
Conversions between real space functions

This appendix will provide transformations between the various real-space functions. A couple of notes before the listing of equations. First, we will be assuming a shape function of $\gamma_0(r) = 1$. This is true for measurements that are sufficiently bulk (i.e. no nanostructures). Second, the correlation number, $N(r)$, will not be mentioned

since it can only be correctly calculated from the partial distributions. Third, the normalization of $g(r)$ provided in the main text will hold here as well.

A.1. Conversions from the reduced pair distribution function, $G(r)$

$$\begin{aligned} R(r) &= rG(r) + 4\pi r^2\rho_0 \\ \rho(r) &= \frac{G(r)}{4\pi r} + \rho_0 \\ G_K(r) &= \frac{\langle b_{coh}\rangle^2}{4\pi r\rho_0}G(r) \\ g(r) &= \frac{G(r)}{4\pi r\rho_0} + 1 \\ D(r) &= \langle b_{coh}\rangle^2 G(r) \\ T(r) &= \langle b_{coh}\rangle^2 \left[G(r) + 4\pi r^2\rho_0\right] \end{aligned} \tag{30}$$

A.2. Conversions from the pair density function, $g(r)$

$$\begin{aligned} R(r) &= 4\pi r^2\rho_0 g(r) \\ \rho(r) &= \rho_0 g(r) \\ G(r) &= 4\pi r\rho_0\left[g(r) - 1\right] \\ G_K(r) &= \langle b_{coh}\rangle^2\left[g(r) - 1\right] \\ D(r) &= 4\pi r\rho_0\langle b_{coh}\rangle^2\left[g(r) - 1\right] \\ T(r) &= 4\pi r\rho_0\langle b_{coh}\rangle^2 g(r) \end{aligned} \tag{31}$$

A.3. Conversions from the radial distribution function, $R(r)$

$$\begin{aligned}
\rho(r) &= \frac{R(r)}{4\pi r^2} \\
G(r) &= \frac{R(r)}{r} - 4\pi r\rho_0 \\
G_K(r) &= \langle b_{coh}\rangle^2 \left[\frac{R(r)}{4\pi r^2\rho_0} - 1\right] \\
g(r) &= \frac{R(r)}{4\pi r^2\rho_0} \\
D(r) &= \langle b_{coh}\rangle^2 \left[\frac{R(r)}{r} - 4\pi r\rho_0\right] \\
T(r) &= \frac{\langle b_{coh}\rangle^2}{r} R(r)
\end{aligned} \tag{32}$$

A.4. Conversions from the number density, $\rho(r)$

$$\begin{aligned}
R(r) &= 4\pi r^2\rho(r) \\
G(r) &= 4\pi r\left[\rho(r) - \rho_0\right] \\
G_K(r) &= \langle b_{coh}\rangle^2 \left[\frac{\rho(r)}{\rho_0} - 1\right] \\
g(r) &= \frac{\rho(r)}{\rho_0} \\
D(r) &= \langle b_{coh}\rangle^2 \left[\frac{\rho(r)}{\rho_0} - 1\right] \\
T(r) &= \langle b_{coh}\rangle^2 4\pi r\rho(r)
\end{aligned} \tag{33}$$

A.5. Conversions from the total radial distribution function, $G_K(r)$

$$
\begin{aligned}
R(r) &= 4\pi r^2 \rho_0 \left[\frac{G_K(r)}{\langle b_{coh} \rangle^2} + 1 \right] \\
\rho(r) &= \rho_0 \left[\frac{G_K(r)}{\langle b_{coh} \rangle^2} + 1 \right] \\
G(r) &= \frac{4\pi r \rho_0}{\langle b_{coh} \rangle^2} G_K(r) \\
g(r) &= \frac{G_K(r)}{\langle b_{coh} \rangle^2} + 1 \\
D(r) &= 4\pi r \rho_0 G_K(r) \\
T(r) &= 4\pi r \rho_0 \left[G_K(r) + \langle b_{coh} \rangle^2 \right]
\end{aligned}
\tag{34}
$$

A.6. Conversions from the differential correlation function, $D(r)$

$$
\begin{aligned}
R(r) &= \frac{r}{\langle b_{coh} \rangle^2} D(r) + 4\pi r^2 \rho_0 \\
\rho(r) &= \frac{D(r)}{4\pi r \langle b_{coh} \rangle^2} + \rho_0 \\
G(r) &= \frac{D(r)}{\langle b_{coh} \rangle^2} \\
G_K(r) &= \frac{D(r)}{4\pi r \rho_0} \\
g(r) &= \frac{D(r)}{4\pi r \rho_0 \langle b_{coh} \rangle^2} + 1 \\
T(r) &= D(r) + \frac{4\pi r^2 \rho_0}{\langle b_{coh} \rangle^2}
\end{aligned}
\tag{35}
$$

A.7. Conversions from the total correlation function, $T(r)$

$$
\begin{aligned}
R(r) &= \frac{rT(r)}{\langle b_{coh}\rangle^2} \\
\rho(r) &= \frac{T(r)}{4\pi r\langle b_{coh}\rangle^2} \\
G(r) &= \frac{T(r)}{\langle b_{coh}\rangle^2} - 4\pi r\rho_0 \\
G_K(r) &= \frac{T(r)}{4\pi r\rho_0} - \langle b_{coh}\rangle^2 \\
g(r) &= \frac{T(r)}{4\pi r\rho_0\langle b_{coh}\rangle^2} \\
D(r) &= T(r) - \frac{4\pi r^2\rho_0}{\langle b_{coh}\rangle^2}
\end{aligned}
\tag{36}
$$

Appendix B
From experimentally observed scattering intensities to differential cross-section

The authors mostly ignored transforming data from measured scattering intensities in section 3 to reciprocal space functions. This appendix will shed light on some of the corrections that are necessary to go from raw measured intensities to a single scattering differential cross-section (DCS), $\frac{d\sigma^s}{d\Omega}$, which can then be used in equation 3. For Rietveld analysis, the level of rigor for corrections is not usually needed for most samples as it is less sensitive to effects such as multiple and inelastic scattering. These effects are frequently seen what is described as the background which is normally fit with a polynomial to reduce its influence on the refinement. However, for real space total scattering measurements, these "minor" effects produce a comparable signal to the reciprocal space representation of local disorder that they must be accounted for. Applying more thorough corrections for data refined with Rietveld provides better

confidence that small features observed arise from the material rather than the experimental setup.

Repeating equation 3

$$S(Q) = \frac{I(Q)}{N\langle b_{coh}\rangle^2} - \frac{\langle b_{tot}^2\rangle - \langle b_{coh}\rangle^2}{\langle b_{coh}\rangle^2}, \tag{37}$$

where $I(Q)$ is **add citation of Egami book**

$$I(Q) = \frac{1}{N}\frac{d\sigma^s}{d\Omega} \tag{38}$$

and N is the number of atoms illuminated. $I(Q)$ can only by found by fully correcting the measured intensity. Proper treatment of total scattering data requires correcting for effects such as attenuation through the sample material and its environment, subtraction of multiple scattering events, and recoil or inelastic effects. That being said, the notation for the various corrections do no have a standard set of definitions. Those will be explained here. The associated measurements for these corrections (e.g. empty container, empty sample environment, normalization) are no longer unusual to perform. Table 1 describes the standard set of measurements required and subscripts that this article will use to refer to them. Additionally, Paalman-Pings **add reference again** developed a detailed notation for the attenuation correction terms whihc will be used. For the measurement of the sample and container combined there are four terms of where the neutron/x-ray was scattered and absorbed in the experiment. For example, the scattering that occurs in only the sample but is attenuated by both the sample and container component is denoted as $A_{s,sc}$. Similarly, the multiple scattering is denoted as M_i for the i^{th} measurement, thus the sample and container are denoted M_{sc}. Finally, the inelastic recoil correction as P_j^{ie} for the j^{th} species, thus the container inelastic correction would be P_c^{ie}. **Add another table for $A_{i,j}$,M_i, and P_j^{ie} and reduce the amount of text in the paragraph. Missing Φ.**

Table 1. *Description of subscripts, i, for measured intensities, $I_i(Q)$, and differential cross sections, $\frac{d\sigma^i}{d\Omega}$, as used below.* ***Change "B" to "e" here and in the equations. Add lines for "sca" and "ca".***

Subscript	Term
s	sample
c	container
a	apparatus
B	background / empty diffractometer
n	normalization

Should the functions be in a table as well? The text is rough/hard to read.

Having the various functions and subscripts definitions in hand, the description of what is actually measured, I_i^E, can be introduced. The experimentally measured intensities for the sample in a container in the sample environment apparatus, the container in the sample environment apparatus, the sample environment apparatus, and the empty diffractometer, respectively, are **Make these $I_i^E(Q,\omega)$**

$$\begin{aligned} I_s^E &= \Phi\left[A_{s,sca}N_s\frac{d^2\sigma^s}{d\Omega d\omega} + A_{c,sca}N_c\frac{d^2\sigma^c}{d\Omega d\omega} + A_{a,sca}N_a\frac{d^2\sigma^a}{d\Omega d\omega} + M_{sca} + \frac{d^2\sigma^B}{d\Omega d\omega}\right] \\ I_c^E &= \Phi\left[A_{c,ca}N_c\frac{d^2\sigma^c}{d\Omega d\omega} + A_{a,ca}N_a\frac{d^2\sigma^a}{d\Omega d\omega} + M_{ca} + \frac{d^2\sigma^B}{d\Omega d\omega}\right] \\ I_a^E &= \Phi\left[A_{a,a}N_a\frac{d^2\sigma^a}{d\Omega d\omega} + M_a + \frac{d^2\sigma^B}{d\Omega d\omega}\right] \\ I_B^E &= \Phi\frac{d^2\sigma^B}{d\Omega d\omega} \end{aligned} \tag{39}$$

Notice that the double-differential cross-section term appears in these equations with $\hbar\omega$ being the energy loss. For the ultimate goal of producing a suitable reciprocal space function, one must integrate over ω to obtain the energy-integrated DCS, we would simply have **Make P^{ie} explicit here**

$$\frac{d\sigma^i}{d\Omega} = \int \frac{d^2\sigma^i}{d\Omega d\omega} d\omega \tag{40}$$

The technique is referred to as total scattering because of this integral across energy transfer. This is not the same as the elastic scattering which can only be properly measured when the incident and final energy of the probe are known. Rietveld analysis has difficulties when the experimenter forgets this point. **does the set of equations with ω need a different left hand side from the ones just below here?**

Performing the integral yeilds the set of equations **Make these** $I_i^E(Q)$

$$\begin{aligned}
I_s^E &= \Phi\Big[A_{s,sca}N_s[\tfrac{d\sigma^s}{d\Omega}+P_s^{ie}]+A_{c,sca}N_c[\tfrac{d\sigma^c}{d\Omega}+P_c^{ie}]+A_{a,sca}N_a[\tfrac{d\sigma^a}{d\Omega}+P_a^{ie}]+M_{sca}+\tfrac{d\sigma^B}{d\Omega}\Big]\\
I_c^E &= \Phi\Big[A_{c,ca}N_c[\tfrac{d\sigma^c}{d\Omega}+P_c^{ie}]+A_{a,ca}N_a[\tfrac{d\sigma^a}{d\Omega}+P_a^{ie}]+M_{ca}+\tfrac{d\sigma^B}{d\Omega}\Big]\\
I_a^E &= \Phi\Big[A_{a,a}N_a[\tfrac{d\sigma^a}{d\Omega}+P_a^{ie}]+M_a+\tfrac{d\sigma^B}{d\Omega}\Big]\\
I_B^E &= \Phi\tfrac{d\sigma^B}{d\Omega}
\end{aligned} \tag{41}$$

Solving each of the equations above for the respective DCS provides:

$$\begin{aligned}
\tfrac{d\sigma^s}{d\Omega} &= \tfrac{1}{A_{s,sca}N_s}\quad \Big[\tfrac{1}{\Phi}(I_s^E-\Phi\tfrac{d\sigma^B}{d\Omega})-M_{sca}-\Big[A_{c,sca}N_c\tfrac{d\sigma^c}{d\Omega}+P_c^{ie}\Big]-\Big[A_{a,sca}N_a\tfrac{d\sigma^a}{d\Omega}+P_a^{ie}\Big]\Big]-P_s^{ie}\\
\tfrac{d\sigma^c}{d\Omega} &= \tfrac{1}{A_{c,ca}N_c}\quad \Big[\tfrac{1}{\Phi}(I_c^E-\Phi\tfrac{d\sigma^B}{d\Omega})-M_{ca}-\Big[A_{a,ca}N_a[\tfrac{d\sigma^a}{d\Omega}+P_a^{ie}]\Big]\Big]-P_c^{ie}\\
\tfrac{d\sigma^a}{d\Omega} &= \tfrac{1}{A_{a,a}N_a}\quad \Big[\tfrac{1}{\Phi}(I_a^E-\Phi\tfrac{d\sigma^B}{d\Omega})-M_a\Big]-P_a^{ie}\\
\tfrac{d\sigma^B}{d\Omega} &= \tfrac{1}{\Phi}I_B^E
\end{aligned} \tag{42}$$

Reducing the equations into terms that only involve the corrections and the measured intensities, the sample DCS is

$$\begin{aligned}
\tfrac{d\sigma^s}{d\Omega} = \tfrac{1}{A_{s,sca}N_s}\quad &\Big[\tfrac{1}{\Phi}(I_s^E-I_B^E)-M_{sca}\\
&-\tfrac{A_{c,sca}}{A_{c,ca}}\Big[\tfrac{1}{\Phi}(I_c^E-I_B^E)-M_{ca}-\tfrac{A_{a,ca}}{A_{a,a}}[\tfrac{1}{\Phi}(I_a^E-I_B^E)-M_a]\Big]\\
&-\tfrac{A_{a,sca}}{A_{a,a}}\Big[\tfrac{1}{\Phi}(I_a^E-I_B^E)-M_a\Big]\Big]-P_s^{ie}
\end{aligned} \tag{43}$$

the container DCS is

$$\tfrac{d\sigma^c}{d\Omega} = \tfrac{1}{A_{c,ca}N_c}\quad \Big[\tfrac{1}{\Phi}(I_c^E-I_B^E)-M_{ca}-\tfrac{A_{a,ca}}{A_{a,a}}[\tfrac{1}{\Phi}(I_a^E-I_B^E)-M_a]\Big]-P_c^{ie} \tag{44}$$

and the sample environment apparatus DCS is

$$\tfrac{d\sigma^a}{d\Omega} = \tfrac{1}{A_{a,a}N_a}\quad \Big[\tfrac{1}{\Phi}(I_a^E-I_B^E)-M_a\Big]-P_a^{ie} \tag{45}$$

The keen reader will notice that the normalization term, Φ, has not been made explicit. This differs based on the probe used. For neutron diffraction, vanadium is an ideal material due to many reasons but the main one being that it has a small coherent scattering length, implying that the distinct scattering signal is small compared to

the self-scattering and thus has a relatively smooth diffraction pattern. Since self-scattering does not vary much with Q or 2θ, the differential cross section is essentially $\frac{d\sigma^v}{d\Omega} \approx \frac{\sigma^v_{tot}}{4\pi} = \langle b^2_v \rangle$ from Eq. 48. For more detail on the use of vanadium, we refer the reader to Section 3.8.1 of GUDRUN (Soper, 2010).

Thus, an additional experimental measurement is needed to characterize the normalization term **Add a break after the first line of this equation with some additional words**

$$\begin{aligned} I^E_n &= \Phi\Big[A_{n,n}N_n[\tfrac{d\sigma^n}{d\Omega} + P^{ie}_n] + M_n + \tfrac{d\sigma^B}{d\Omega}\Big] \\ &= \Phi\Big[A_{n,n}N_n[\langle b^2_v\rangle + P^{ie}_n] + M_n + \tfrac{d\sigma^B}{d\Omega}\Big] \\ &= \Phi\Big[A_{n,n}N_n[\langle b^2_v\rangle + P^{ie}_n] + M_n\Big] + \Phi\tfrac{d\sigma^B}{d\Omega} \\ &= \Phi\Big[A_{n,n}N_n[\langle b^2_v\rangle + P^{ie}_n] + M_n\Big] + I^E_B \end{aligned} \tag{46}$$

Solving for Φ gives

$$\Phi = \frac{I^E_n - I^E_B}{[A_{n,n}N_n[\langle b^2_v\rangle + P^{ie}_n] + M_n]} \tag{47}$$

Which can be used in the equations above.

Need a closing statement

Appendix C
Calculating the normalized Laue term

There is often confusion when determining the normalized Laue term of equation 4. In his book, (Lovesey, 1986) introduced quantities related to the total cross section of the material,

$$\sigma_{tot} = 4\pi\langle b^2_{tot}\rangle \tag{48}$$

and the coherent cross section,

$$\sigma_{coh} = 4\pi\langle b_{coh}\rangle^2 \tag{49}$$

These are the terms that appear in the normalized Laue with the factor of 4π cancelled out. It must be pointed out that $\langle\sigma_{coh}\rangle \neq 4\pi\langle b_{coh}\rangle^2$, but Lovesey's notation obscures this fact. Being more explicit it is straightforward to calculate the terms as originally intended. First we introduce a normalized concentration

$$c_\alpha = N_\alpha / N \tag{50}$$

where N_α is the number of atoms of type α and $N = \sum_\alpha N_\alpha$. This provides for the normalization that $\sum_\alpha c_\alpha = 1$. Then the two quantities needed in the normalized Laue term are simply

$$\langle b_{tot}^2\rangle = \sum_\alpha c_\alpha b_{tot,\alpha}^2 = \frac{1}{4\pi}\sum_\alpha c_\alpha \sigma_{tot,\alpha} \tag{51}$$

and

$$\langle b_{coh}\rangle^2 = \left(\sum_\alpha c_\alpha b_{coh,\alpha}\right)\left(\sum_\alpha c_\alpha b_{coh,\alpha}^*\right) \tag{52}$$

This formulation of $\langle b_{coh}\rangle^2$ makes more explicit that the complex scattering lengths, with sign, are averaged. Unique to neutron measurements, this can lead to materials where the normalized Laue term becomes infinite because of atoms with a negative scattering length.

An additional complication is found when the $\langle b_{tot}^2\rangle$ is calculated. Since $1 barn = 100 fm^2$, people often calculate $\langle b_{tot}^2\rangle$ by simply dividing by 4π and ignoring the units. While the factor of 100 will cancel out in the normalized Laue term, the values of the individual terms will be listed in units of $10 fm$ (or deka-femto-meters) rather than fm. Tables 1 and 2 show example calculations for the example materials.

Table 1. *Table of scattering lengths for the example materials taken from (Sears, 1992).*

		b_{coh} (fm)		
Atom	b_{tot} (fm)	real	imag	length
Ar	2.3313	1.909	0.0	1.909
Mn	4.1363	-3.73	0.0	3.73
O	5.8032	5.803	0.0	5.803

Table 2. *Calculated values for the normalized Laue term shown with fixed precision. Note that the normalized Laue term is not necessarily zero for monotonic materials.*

Material	$\langle b_{tot}^2\rangle$ (fm^2)	$\langle b_{coh}\rangle^2$ (fm^2)	L
Ar	5.435	3.644	0.491
MnO	25.393	1.074	22.636

Appendix D
Determining number density

Often when processing or analyzing data, the average number density is treated as a freely adjustable parameter. Here we demonstrate how to calculate it and give guidance on reasonable limits. The total number of atoms scattering, $N = \rho_0 V$, can be calculated by the number density and illuminated volume of the sample and is needed in order to get an absolute scaling factor for $S(Q)$. Even when the mass density is known well, there is a packing fraction, $f \in (0, 1]$, used to convert from mass density to number density and the illuminated volume is not known with high precision.

It should be noted that the average number density for a crystalline sample is often phrased in terms of the number of atoms per unit cell, called the Z-parameter, and the unit cell volume. Using standard crystallographic conventions (Giacovazzo, 1992)

$$\rho_0 = \frac{Z}{\vec{a} \cdot (\vec{b} \times \vec{c})} \tag{53}$$

For materials that cannot be represented by crystallographically, this will have to be determined from the mass density ρ_m

$$\rho_0 = f \frac{\rho_m N_A}{\sum_\alpha c_\alpha m_\alpha} \tag{54}$$

Where N_A is Avogadro's number, m_α is the atomic mass, and c_α is the normalized concentration of the α element or the atomic fraction as defined in Appendix C. The packing fraction, f, can be adjusted between **(Kate need reasonable lower limit)** and 1, being a single crystal. This is normally how crystalline samples number density is determined as well. The number density is also required by absorption and multiple scattering corrections as described in Appendix B. Some analysis software allow for scaling the data which should ideally be 1. An alternative to this approximation is

to properly measure the volume by via displacement in a fluid that the material does not react with and is insoluble. However, it will likely be difficult to recover a powder from this type of measurement so it is recommended to be done after the scattering measurement is completed.

Appendix E
Partial structure functions

To use the prevalent Faber-Ziman partial structure functions, one must first define weights (Faber & Ziman, 1965; Suck *et al.*, 1993; Egami & Billinge, 2012)

$$W_{\nu\mu} = c_\nu c_\mu \frac{b_{coh,\nu} b_{coh,\mu}}{\langle b_{coh}\rangle^2} = \frac{N_\nu N_\mu}{N^2} \frac{b_{coh,\nu} b_{coh,\mu}}{\langle b_{coh}\rangle^2} \tag{55}$$

which are normalized such that $\sum_\nu \sum_\mu W_{\nu\mu} = 1$. Note that the same symbol is used with an alternate normalization in some communities with $\sum_\nu \sum_\mu W_{\nu\mu} = \langle b_{coh}\rangle^2$. The Faber-Ziman partial structure functions which are related to the total scattering structure factor

$$S(Q) = \sum_{\nu\mu} W_{\nu\mu} A_{\nu\mu}(Q) \tag{56}$$

$A_{\nu\mu}(Q) = S_{\nu\mu}(Q)$ in the nomenclature that Egami uses. The benefit of the normalization of $S_{\nu\mu}(Q)$ is that it has similar asymptotes as $S(Q)$ with

$$\lim_{Q\to\infty} A_{\nu\mu}(Q) = 1 \tag{57}$$

and

$$\lim_{Q\to 0} A_{\nu\mu}(Q) = W_{\nu\mu} \tag{58}$$

where the $\langle b_{coh}\rangle^2$ is the average scattering length for the material, and the numerator is the average scattering length for the atoms contributing to the partial.

Then it is straightforward to define a partial reduced pair-distribution function, as

$$G_{\nu\mu}(r) = \frac{2}{\pi}\int_0^\infty Q[A_{\nu\mu}(Q) - 1]sin(Qr)dQ \tag{59}$$

which observes a summation rule of

$$G(r) = \sum_\nu \sum_\mu W_{\nu\mu} G_{\nu\mu}(r) \tag{60}$$

The other real space correlation functions follow analogous forms.

To clarify a related point, difference correlation functions are a distinct concept. Instead of being the correlation of two atomic species, it is all correlations with an atom of type ν at the origin. In other words

$$G_\nu(r) = \sum_\mu \frac{c_\mu b_{coh,\mu}}{\langle b_{coh}\rangle^2} G_{\nu\mu}(r) \tag{61}$$

which follows the summation rule

$$G(r) = \sum_\nu \frac{c_\nu b_{coh,\nu}}{\langle b_{coh}\rangle^2} G_\nu(r) \tag{62}$$

For a more detailed description see (Egami & Billinge, 2012) sections 3.1 and 3.2.

For a two-atom system with atoms labeled α and β, the summation rule for the weights in equation 55, is

$$W_{\alpha\alpha} + 2W_{\alpha\beta} + W_{\beta\beta} = 1 \tag{63}$$

For a monotonic system, there are no partial functions. See table 1 for explicit calculation of the values. Figure 6 shows the partial $G(r)$.

Table 1. *Weights, $W_{\nu\mu}$ for partials for the materials chosen. The atom listed first in the chemical formula is α and the second is β.*

Material	$W_{\alpha\alpha}$	$W_{\alpha\beta}$	$W_{\beta\beta}$
Ar	1.000	n/a	n/a
MnO	3.238	5.037	7.836

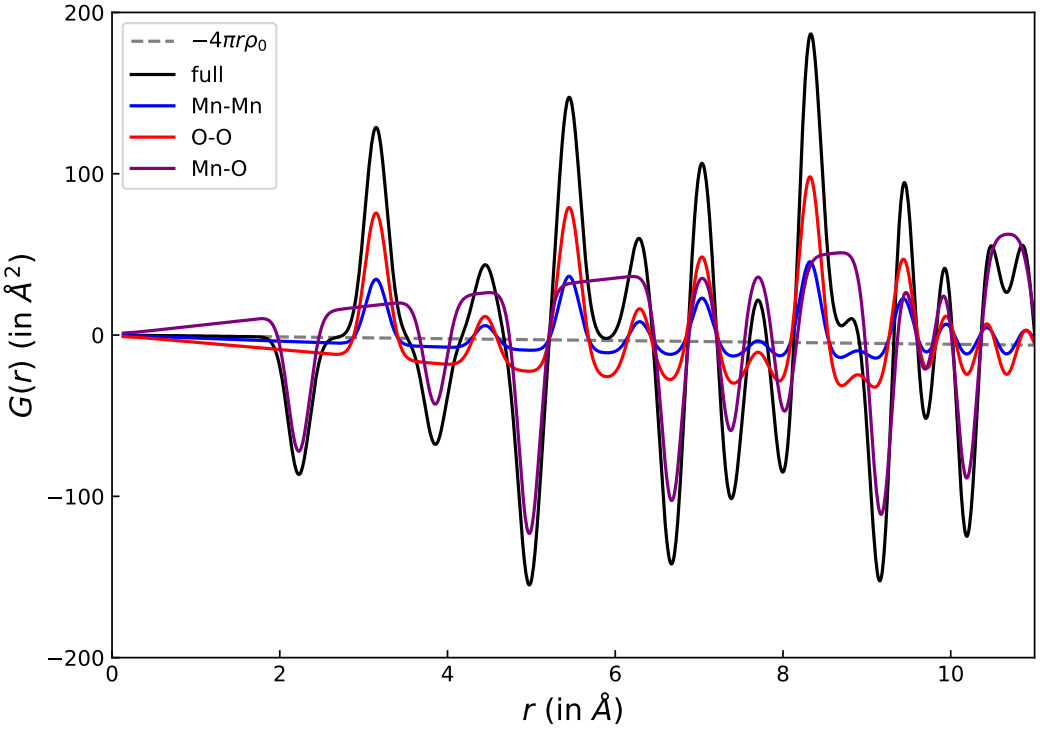

Fig. 6. Partial reduced pair distribution functions for MnO.

Acknowledgements

Work at ORNL was sponsored by the Scientific User Facilities Division, Office of Basic Energy Sciences, US Department of Energy. **Need acknowledgement for Matt and Joerg who were awesome and patient.**

References

Azaroff, L. V. (1968). *Elements of X-ray crystallography*. New York: McGraw-Hill.

Bhatia, A. & Thornton, D. (1970). *Physical Review B*, **2**(8), 3004.

Billinge, S. J. L. (1992). *Local Atomic Structure and Superconductivity of $Nd_{2-x}Ce_xCuO_{4-y}$: A Pair Distribution Function Study*. Ph.D. thesis, University of Pennsylvania.

Billinge, S. J. L. & Egami, T. (1993). *Physical Review B*, **47**(21), 14386.

Debye, P. (1915). *Annalen der Physik*, **351**(6), 809–823.

Egami, T. & Billinge, S. J. L. (2012). *Underneath the Bragg peaks : structural analysis of complex materials*. San Diego California, USA: Pergamon.

Egelstaff, P. A. (1992). *An introduction to the liquid state*. Oxford New York: Clarendon Press Oxford University Press.

Faber, T. & Ziman, J. (1965). *Philosophical Magazine*, **11**(109), 153–173.

Farrow, C., Juhas, P., Liu, J., Bryndin, D., Božin, E., Bloch, J., Proffen, T. & Billinge, S. (2007). *Journal of Physics: Condensed Matter*, **19**(33), 335219.

Farrow, C., Juhás, P., Liu, J., Bryndin, D., Bozin, E., Bloch, J., Proffen, T. & Billinge, S., (2016). Pdfgui user guide, 2016.
URL: *http://www.diffpy.org/doc/pdfgui/pdfgui.pdf*

Farrow, C. L. & Billinge, S. J. L. (2009). *Acta Crystallographica Section A Foundations of Crystallography*, **65**(3), 232239.

Giacovazzo, C. (1992). *Fundamentals of crystallography*. Chester, England Oxford New York: International Union of Crystallography Oxford University Press.

Gilbert, B. (2008). *Journal of Applied Crystallography*, **41**(3), 554–562.

Guinier, A. & Fournet, G. (1955). *Small-Angle Scattering of X-rays*. New York: Wiley & Sons, NY. Translated by C.B.Walker.

Hannon, A., Howells, W. & Soper, A. (1990). In *Inst. Phys. Conf. Ser*, vol. 107, pp. 193–211.

Hoover, W. G. (1985). *Physical Review A*, **31**(3), 1695–1697.
URL: *http://link.aps.org/doi/10.1103/PhysRevA.31.1695*

Jeong, I.-K., Heffner, R., Graf, M. & Billinge, S. (2003). *Physical Review B*, **67**(10), 104301.

Jeong, I.-K., Proffen, T., Mohiuddin-Jacobs, F. & Billinge, S. J. (1999). *The Journal of Physical Chemistry A*, **103**(7), 921–924.

Juhás, P., Davis, T., Farrow, C. L. & Billinge, S. J. (2013). *Journal of Applied Crystallography*, **46**(2), 560–566.

Keen, D. A. (2001). *Journal of Applied Crystallography*, **34**(2), 172177.

Kodama, K., Iikubo, S., Taguchi, T. & Shamoto, S. i. (2006). *Acta Crystallographica Section A: Foundations of Crystallography*, **62**(6), 444–453.

Lovesey, S. W. (1986). *Theory of neutron scattering from condensed matter*. Oxford Oxfordshire: Clarendon Press.

Nosé, S. (1984). *The Journal of Chemical Physics*, **81**(1), 511–519.
URL: *http://scitation.aip.org/content/aip/journal/jcp/81/1/10.1063/1.447334*

Olds, D., Saunders, C. N., Peters, M., Proffen, T., Neuefeind, J. & Page, K. (2018). *Journal of Applied Crystallography*, **accepted**.

Olds, D., Wang, H.-W. & Page, K. (2015). *Journal of Applied Crystallography*, **48**(6), 1651–1659.

Page, K., White, C. E., Estell, E. G., Neder, R. B., Llobet, A. & Proffen, T. (2011). *Journal of Applied Crystallography*, **44**(3), 532–539.

Peterson, P. F., Bozin, E. S., Proffen, T. & Billinge, S. J. L. (2003). *Journal of Applied Crystallography*, **36**(1), 5364.

Plimpton, S. (1995). *Journal of Computational Physics*, **117**(1), 1 – 19.
URL: *http://www.sciencedirect.com/science/article/pii/S002199918571039X*

Plimpton, S. J., (2018). Large-scale atomistic/molecular massively parallel simulator (lammps) website.
URL: *http://lammps.sandia.gov/*

Proffen, T. & Billinge, S. (1999). *Journal of Applied Crystallography*, **32**(3), 572–575.

Qiu, X., Božin, E. S., Juhas, P., Proffen, T. & Billinge, S. J. (2004). *Journal of Applied Crystallography*, **37**(1), 110–116.

Sasaki, S., Fujino, K. & Takéuchi, Y. (1979). *Proceedings of the Japan Academy, Series B*, **55**(2), 43–48.

Sears, V. F. (1992). *Neutron news*, **3**(3), 26–37.

Soper, A. (1989). *ATLAS manual, Neutron Science Division, Rutherford Appleton Laboratory, Chilton, OX11 0QX*.

Soper, A. K., (2010). Gudrun and gudrunx: Programs for correcting raw neutron and x-ray diffraction data to differential scattering cross section.
URL: *https://www.isis.stfc.ac.uk/OtherFiles/Disordered%20Materials/Gudrun-Manual-2017-10.pdf*

Suck, J. B., Raoux, D., Chieux, P. & Riekel, C. (1993). *Proceedings of the ILL/ESRF Workshop on Methods in the Determination of Partial Structure Factors of Disordered Matter by Neutron and Anomalous X-Ray Diffraction, Grenoble, France, 10-11 September 1992*. Singapore River Edge, N.J: World Scientific.

Thorpe, M., Levashov, V., Lei, M. & Billinge, S. J. (2002). In *From semiconductors to proteins: beyond the average structure*, pp. 105–128. Springer.

Tucker, M., Dove, M., Goodwin, A., Keen, D. A., Playford, H. & Slawinski, W. A., (2017). Rmcprofile user manual. Code version 6.7.0.

Tucker, M. G., Keen, D. A., Dove, M. T., Goodwin, A. L. & Hui, Q. (2007). *Journal of Physics: Condensed Matter*, **19**(33), 335218.

Verlet, L. (1967). *Phys. Rev.* **159**, 98–103.
URL: *https://link.aps.org/doi/10.1103/PhysRev.159.98*

Wagner, C. (1985). *Journal of non-crystalline solids*, **76**(1), 29–42.

Wang, H.-W., Fanelli, V. R., Reiche, H. M., Larson, E., Taylor, M. A., Xu, H., Zhu, J., Siewenie, J. & Page, K. (2014). *Review of Scientific Instruments*, **85**(12), 125116.

Warren, B. E. (1990). *X-ray diffraction*. New York: Dover Publications.

Yarnell, J., Katz, M., Wenzel, R. G. & Koenig, S. (1973). *Physical Review A*, **7**(6), 2130.

Zhang, J. (1999). *Physics and Chemistry of Minerals*, **26**(8), 644–648.

Synopsis

A presentation of the derivations of and relationships between many of the commonly employed functional forms of real and reciprocal space data employed by the worldwide total scattering community.